ChemPubSoc Europe

DOI: 10.1002/chem.201405239

CHEMISTRY
A European Journal
Communication

Organic Electronics

Synthesis and Characterization of a Helicene-Based Imidazolium Salt and Its Application in Organic Molecular Electronics

Jan Storch,*[a] Jaroslav Zadny,[a] Tomas Strasak,[a] Martin Kubala,[b] Jan Sykora,[a] Michal Dusek,[c] Vladimir Cirkva,[a] Pavel Matejka,[d] Milos Krbal,[e] and Jan Vacek*[f]

Abstract: Herein we demonstrate the synthesis of a helicene-based imidazolium salt. The salt was prepared by starting from racemic 2-methyl[6]helicene, which undergoes radical bromination to yield 2-(bromomethyl)[6]helicene. Subsequent treatment with 1-butylimidazole leads to the corresponding salt 1-butyl-3-(2-methyl[6]helicenyl)-imidazolium bromide. The prepared salt was subsequently characterized by using NMR spectroscopy and X-ray analysis, various optical spectrometric techniques, and computational chemistry tools. Finally, the imidazolium salt was immobilized onto a SiO_2 substrate as a crystalline or amorphous deposit. The deposited layers were used for the development of organic molecular semiconductor devices and the construction of a fully reversible humidity sensor.

Imidazole derivatives and imidazolium salts are functional molecules with a broad spectrum of applications in physical, chemical, and biochemical research and technology development. One of the main focuses of interest is the design of imidazolium salts, functional derivatives, ionic liquids, and polymers resulting in novel species with tailored physicochemical properties leading to better stability, solubility, and higher applicability in analytical chemistry, materials science, and biomedicine in general. The broad spectrum of imidazole and imidazolium salt applications in various fields have been described by many authors. Specifically, the applications for the preparation of polymers,[1] modification of solid surfaces and catalysis,[2] formation of carbonic species and supramolecular systems,[3] biomedicine applications and the use of imidazole derivatives in therapeutic approaches,[4] and the application of imidazolium salts as ionic liquids[5] can be found in the respective review papers.

In this paper we focused on the substitution of the imidazolium cation with [6]helicene. The hypothesis for the preparation of the imidazolium-helicene hybrid was based on improving the properties of helicene for surface immobilization, enhancing its solubility in more polar solvents and last, but not least, finding advanced applications for helicenes in the development of electronic devices.

The helicene and its derivatives were shown to be effective in the development of materials with chiroptical properties useful for molecular-based electronic applications;[6–8] for example, the recently published study focused on 1-aza[6]helicene.[9] Other studies were focused on the interaction of helicenes with biomacromolecules and the preparation of helicene polymeric structures. In terms of the optical properties of helicenes, selected derivatives also have potential as fluorescent active probes and dyes. In comparison to imidazolium salts and their applications, the number of helicene modifications is still rather limited. An overview of selected applications of helicene derivatives, conjugates, and their salts can be found in Table S1 (see the Supporting Information).

A helicene-based imidazolium salt was synthesized by starting from 2-methyl[6]helicene, which undergoes radical bromination to give 2-(bromomethyl)[6]helicene **1**. The treatment of **1** with 1-butylimidazole in methyl isobutyl ketone gave racemic **2** as a stable crystalline compound with an 80% yield (Figure 1). For details on the synthesis and structural data, see Section 2 in the Supporting Information.

Good single crystals of **2** suitable for X-ray diffraction studies were obtained from CH_2Cl_2/acetonitrile solution. The compound crystallizes in the space group *Pbca*, which indicates the presence of both helicene enantiomers (P and M type) in the crystal lattice. The independent part of the unit cell is occupied by a single molecule (Section 2 in the Supporting Information). The [6]helicene and imidazolium moieties tend to assemble separately forming alternating domains along the crystallographic *c* axis (Figure 2). There are two remarkable kinds

[a] *Dr. J. Storch, Dr. J. Zadny, Dr. T. Strasak, Dr. J. Sykora, Dr. V. Cirkva*
Institute of Chemical Process Fundamentals of the AS CR, v.v.i.
Praha 6,165 02 (Czech Republic)
E-mail: storchj@icpf.cas.cz

[b] *Prof. Dr. M. Kubala*
Department of Biophysics, Faculty of Science, Palacky University
tr. 17. listopadu 12, 77146 Olomouc (Czech Republic)

[c] *Dr. M. Dusek*
Institute of Physics of the ASCR, v. v. i., Cukrovarnicka 10/112
162 00 Praha 6 (Czech Republic)

[d] *Prof. Dr. P. Matejka*
Department of Physical Chemistry, Institute of Chemical Technology
Prague, Technicka 5, 166 28 Prague 6 (Czech Republic)

[e] *Dr. M. Krbal*
Department of General and Inorganic Chemistry, Faculty of Chemical Technology, University of Pardubice
Cs. Legion's sq. 565, Pardubice, 532 10 (Czech Republic)

[f] *Prof. Dr. J. Vacek*
Department of Medical Chemistry and Biochemistry, Faculty of Medicine, Palacky University
Hnevotinska 3, Olomouc, 775 15 (Czech Republic)
E-mail: jan.vacek@upol.cz

Supporting information for this article is available on the WWW under http://dx.doi.org/10.1002/chem.201405239.

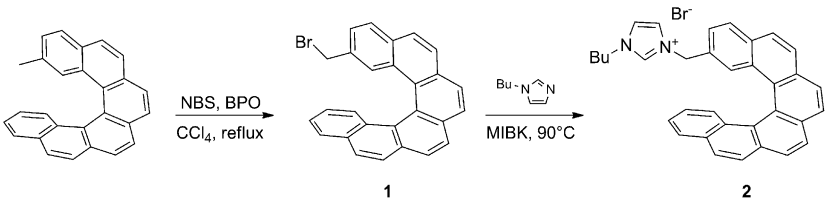

Figure 1. Synthesis of racemic 1-butyl-3-(2-methyl[6]helicenyl)-imidazolium bromide (**2**). NBS = *N*-bromosuccinimide; BPO = benzoyl peroxide; MIBK = methyl isobutyl ketone.

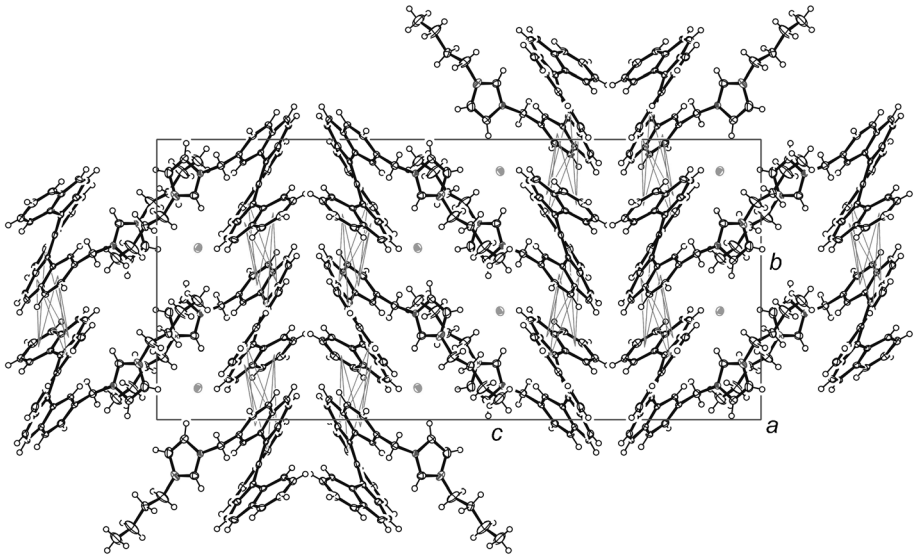

Figure 2. ORTEP projection of molecular packing in the crystal structure of **2**. For a more detailed view, see Figures S1 and S2 in the Supporting Information. π–π Interactions are highlighted.

of interaction within helicene domains. 1) π–π stacking of two adjacent molecules along the *b* axis. P- and M-type helicenes alternate in this direction with interactions between the electron-rich and -poor parts of the helicene subunits (the distance of the interacting aromatic rings is 3.5 Å). 2) A strong CH–π interaction can be found along the *a* axis (CH—aromatic ring distance 1.91 Å).

To obtain insights into the electronic structure of **2**, we performed quantum-chemical calculations using DFT (see Section 3 in the Supporting Information). For evaluating of the effect of the imidazolium subunit on the helicene moiety, we selected 2-methyl[6]helicene as a comparative model. The input geometries were obtained from the crystallographic structures (see previous paragraph) and optimized without any constraints (Figure 3A). HOMO and LUMO representations are shown in Figure 3B,C. The calculated band gap for **2** was found to be 3.92 eV, similar to that computed for 2-methyl[6]helicene (3.96 eV). Kertesz et al. determined the [6]helicene HOMO–LUMO gap value to be 3.99 eV.[10]

When comparing the HOMO orbitals of **2** to the 2-methyl[6]-helicene, the electronic density slightly decreases along the aromatic system toward the imidazolium ring (Figure 3B). This trend follows the distribution of the π-surface in the *y* axis of the helicenes with decreasing HOMO (from −5.53 eV for the 2-methyl[6]helicene to −6.15 eV for **2**) and LUMO levels (from −1.56 eV for the 2-methyl[6]helicene to −2.23 eV for **2**). The natural atomic charges calculated from a natural bond orbital (NBO) analysis are shown in Table S2 (see the Supporting Information). When comparing the computed values of partial charges of corresponding carbon atoms of 2-methyl[6]helicene and **2**, no significant change was observed. The NBO charge of C2 of the 2-methyl[6]helicene (−0.043) was slightly increased compared to **2** (−0.087). The remaining partial charges of the aromatic system stayed almost unchanged. The electron-density isosurface mapped with the electrostatic potential surface of **2** (Figure S3 in the Supporting Information) shows the charge distribution in the molecule. Positive charge is located on the imidazolium ring separated from the helicene by the methylene spacer. The colored surface illustrates a fur-

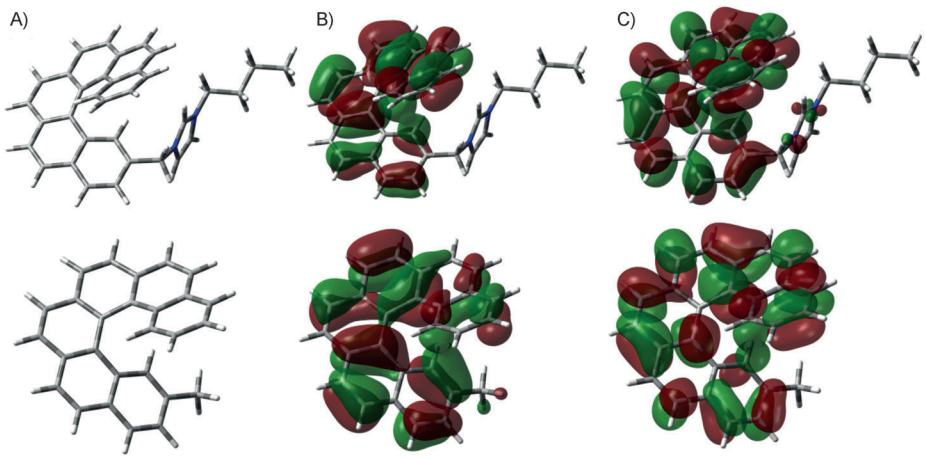

Figure 3. Calculated structures (A), HOMO (B), and LUMO (C) of compound **2** (up) and 2-methyl[6]helicene (down) using the B3LYP/6-31G (d,p) method with the PCM of chloroform.

ther decrease in positive charge along the aromatic system of the [6]helicene (Figure S3 in Supporting Information).

For a comparison of the effect of the imidazolium moiety on the optical and other physicochemical properties of **2**, 1-butyl-3-methyl imidazolium bromide **3** was used in all spectrometric experiments. UV/Vis absorption spectra of **2** and **3** in chloroform were recorded in the wavelength range $\lambda = 250$–800 nm (at shorter wavelengths, the strong absorption of chloroform hinders measurement). Compound **3** is a colorless compound, and its absorption spectrum has a peak at 274 nm with a relatively low extinction coefficient ($\varepsilon = 1100\ cm^{-1}\,M^{-1}$), which is typical for the $n \rightarrow \pi^*$ transition. The presence of the [6]helicene moiety influenced the **2** absorption spectrum considerably (Figure 4A). There are two peaks, the major one located at 266 nm with an extinction coefficient $\varepsilon = 80\ 000\ cm^{-1}\,M^{-1}$, and the lower one with an apparent doublet at $\lambda = 318$ and 328 nm ($\varepsilon = 34\ 000\ cm^{-1}\,M^{-1}$ for both peaks). These values are in line with previously published data for helicene derivatives[11] and are rather typical for $\pi \rightarrow \pi^*$ transitions. The calculated energy of the HOMO–LUMO band gap of **2** corresponding to 316.4 nm is also in a good agreement with the first peak at 318 nm. In fact, the latter peak has a strong vibronic pattern and after careful inspection, at least eight peaks can be identified, which are regularly distributed on the wavenumber scale between 24271 and 34423 cm^{-1} with mutual distances of 1456 cm^{-1} (as determined from a linear fit, $R^2 = 0.997$), pointing to a strong coupling of an electronic transition with this particular vibrational mode of [6]helicene moiety. The last peak of this series located at about $\lambda = 412$ nm ($\varepsilon = 580\ cm^{-1}\,M^{-1}$) is responsible for the yellowish color of the **2** solution.

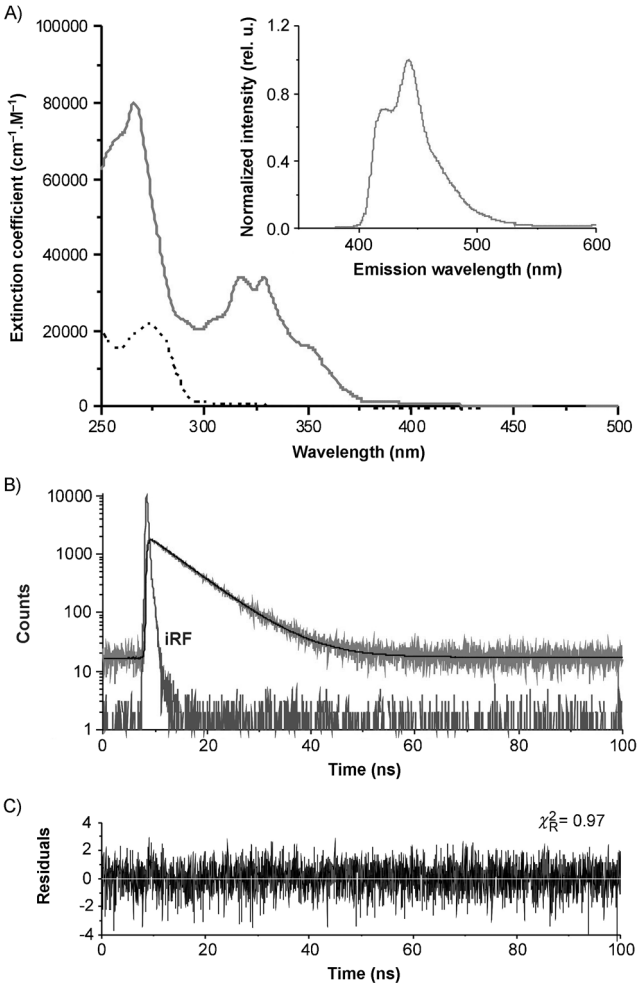

Figure 4. A) Absorption spectra of **2** and **3** (——: **2**; -----: **3**). Inset) Normalized emission spectrum of **2** recorded with excitation at 318 nm. B) Fluorescence decay of **2** (top) upon excitation by a pulsed LED at 308 nm (IRF—bottom). The black line represents the best single-exponential fit and the bottom graph (C) shows the distribution of residuals. The extinction coefficient of **3** in panel (A) is displayed magnified by a factor of 20 for better visibility.

Compound **3** in chloroform yielded no apparent fluorescence upon excitation at 274 nm and was not examined further. On the other hand, compound **2** yielded a blue fluorescence with a quantum yield $QY = 0.021$. The emission peak also exhibits a vibronic structure with a minor peak at $\lambda =$ 420 nm and a major peak at $\lambda = 442$ nm (further vibrational satellites are only barely visible). Notably, the shape of the emission spectrum was identical for excitation at $\lambda = 318$, 328, and 350 nm, which suggests that the emission comes from the same (fully relaxed) electronic excited state (inset in Figure 4A).

The fluorescence decay of **2** was determined by using a time-correlated single photon counting (TCSPC) method. The kinetics could be easily fitted to a single-exponential decay function with $\tau = 6.52 \pm 0.03$ ns, yielding a $\chi^2_R = 0.97$ and a random distribution of residuals (Figure 4B,C). A comparison of the mean fluorescence lifetime and fluorescence *QY* enabled us to calculate the rate constants for the radiative (k_R) and non-radiative (k_N) de-excitation processes, as described in Section 4 in the Supporting Information. The calculation gave $k_R = 3.2 \times 10^6\ s^{-1}$ and $k_N = 150 \times 10^6\ s^{-1}$.

FT Raman spectra of **2** and **3** were compared mutually (Figure 5). The bands of the [6]helicene moiety are dominant in the FT Raman spectrum of **2**. The strongest band at 1357 cm^{-1} is a typical strong band of a ring-breathing (D-type) mode of the [6]helicene skeleton as described both experimentally and by DFT calculations for 2-Br-hexahelicene.[12] There are strong similarities among the Raman responses of [6]helicene, coronene, and graphene; the graphitic G- and D-lines are usually found in [6]helicene derivatives at approximately 1600 and 1350 cm^{-1}, respectively. With **2**, the band of the G-type mode is relatively weak at 1601 cm^{-1}, but it is stronger than the fea-

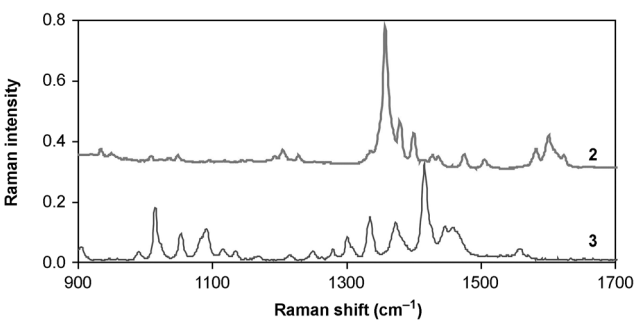

Figure 5. FT Raman spectra of **2** and **3**.

tures of the butyl-imidazolium part of the **2** molecule. Nevertheless, many bands of **3** can be observed in the spectrum of **2** as very weak features, frequently without a significant frequency shift (Figure 5). A detailed comparison of band positions and their assignment based on published data[13–15] shows that there is practically no effect of the helicene moiety on the butyl skeleton, whereas slight shifts in the bands assigned to the imidazolium ring are evident, which indicates the influence of the [6]helicene skeleton on the electron density on the imidazolium ring.

After a complex evaluation of the optical properties of **2** in solution, we focused on the surface immobilization of **2** by spin-coating and its application in the preparation of conjugated molecular semiconductors. To examine the applicability of the spin-coated **2**, we conducted d.c. electrical conductivity measurements (for details on the experimental cell construction, see Figure S4 in the Supporting Information) over the range of temperatures from 30 to 160 °C in the dark and upon light exposure with annealed samples at 100 or 190 °C.

Figure 6 shows the effect of temperature on I-V curves (in the dark) of the annealed (at 100 °C) spin-coated thin film of **2**. The experimental data clearly demonstrate the substantial increase in current for four orders of magnitude from 3×10^{-10} to 2×10^{-6} A under the constant voltage of −28 V in the selected temperature range (the activation energy is 0.7 eV). The room-temperature currents for spin-coated **2** were nearly the same as for spin-coated 1-aza[6]helicene.[9] However, in our tested device the spacing between Au electrodes was 1 cm, in contrast to the 10 μm used with 1-aza[6]helicene.[9] Since the other dimensions (film thickness and length of Au electrodes) were identical in both devices, we can assume from the formula $R=\rho\times[l/(h\times w)]$, in which R is resistance, ρ is conductivity, l is spacing between electrodes, h is film thickness and w is length of Au electrode, that spincoated films of **2** are about three orders of magnitude more conductive than the 1-aza[6]-helicene film.[9]

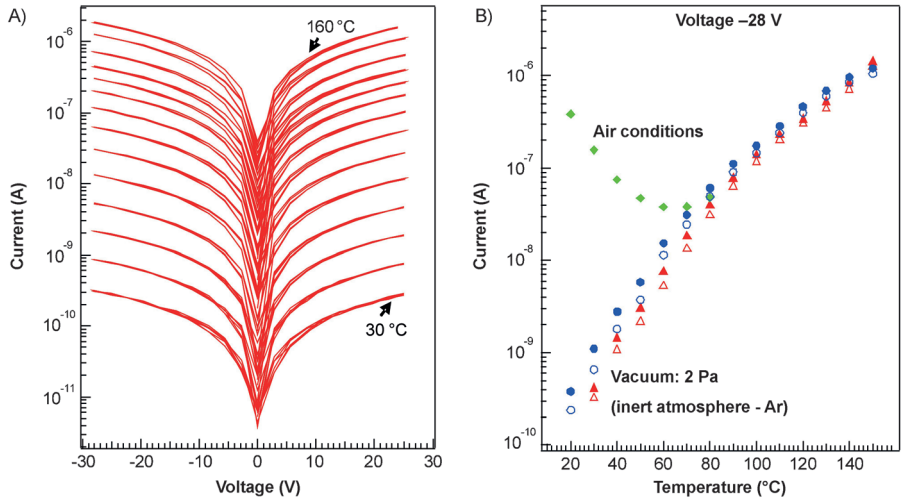

Figure 6. A) I-V curves (in the dark) of the annealed (at 100 °C) spincoated thin film of **2** in the temperature range of 30–160 °C. B) Dependence of current on temperature at voltage −28 V for spincoated **2** film annealed at 100 °C (▲) and 190 °C (●) measured at 2 Pa under a constant flow of Ar. The open and filled symbols represent current(T) in the dark and upon exposure to light, respectively. ◆ represents current(T) measured at ambient conditions.

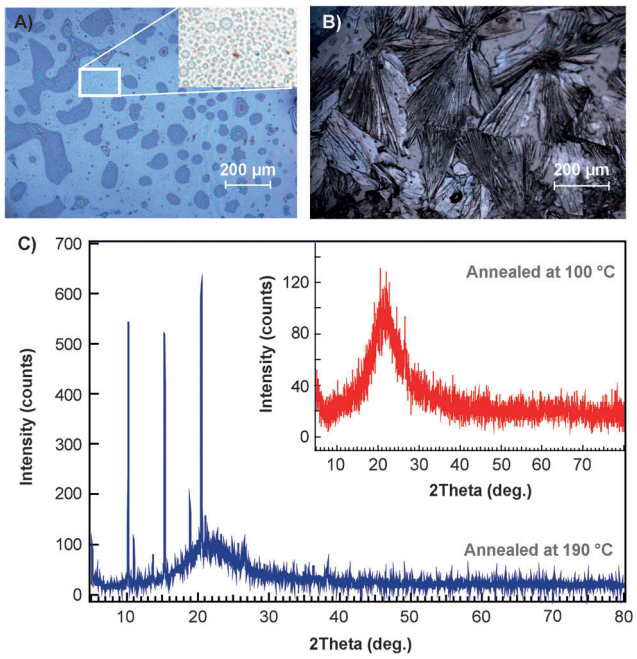

Figure 7. Micrographs of the amorphous (A) and crystalline (B) spincoated thin-film surface of **2**. For A: The darker zones represents a peeling off (not cracking) of the sample from the SiO_2 substrate. The insert is a picture of the magnified area that demonstrates domain formation at the micron scale. C) Bragg diffractions of the thin films.

With respect to the fact that annealing the thin film at 190 °C improves the conductivity of the sample (Figure 6B), we examined both samples (100 vs. 190 °C) using Bragg diffraction and optical microscopy to investigate possible structural modifications of the spincoated **2** film. The microscopic structures of the annealed spincoated **2** at 100 and 190 °C are clearly seen in Figure 7A,B, respectively. From the macroscopic point of view, the annealed sample at 100 °C appears homogeneous, nevertheless it contains domains with the size of a few microns (see inset in Figure 7A). On the other hand, the annealed sample at 190 °C is mostly composed of crystals with a size of several hundred microns, which overlap each other, and thus they create a connected path across the sample between the two gold electrodes. The amorphous or crystalline character of both samples was confirmed by Bragg diffraction (Figure 7C). Since the crystalline phase enhances the conductivity of the studied material, it is crucial to know the onset of the crystallization. To close this gap, using a heating stage in combination with an optical microscope for

monitoring the crystal growth, we found that obvious crystallization begins at 160 °C.

It is important to emphasize that the spincoated **2** thin films are sensitive to exposure to UV light (see Figure 6B and Figure S5 in the Supporting Information). In our experiment we exposed the device to a polychromatic light source through a filter to efficiently cut off the IR radiation and thus to prevent additional sample heating. The overall UV intensity that impacted the sample was approximately 2 mW cm^{-2} as determined experimentally. When the device was illuminated, the value of current rapidly increased. It needs to be stressed that the UV light sensitivity of spin-coated **2** is stronger in the temperature range 20 to 50 °C. Similar effects important for organic phototransistors have been observed in other cases, for example, pentacene-based OFET.[16,17]

Finally, it has been reported that organic field-effect transistors based on pure 1-aza[6]helicene dissolved in toluene are unstable under ambient conditions.[9] Here in this paper, we recorded I-V curves (in the dark) under ambient conditions and compared them with previous measurements (at 2 Pa + Ar atmosphere). It was observed that the current is about three orders of magnitude higher (3×10^{-10} to 4×10^{-7} A) for measurements at ambient conditions under a constant voltage of −28 V (Figure 6B, ◆).

We propose that the current increase is caused by air humidity. Crystalline (dry) imidazolium itself has a strong affinity to being dissolved in the moisture in the air. Similarly, the imidazolium component in the spin-coated **2** can be affected by the humidity in the air and thus may change the material's conductivity. Nevertheless, when a cell with the sample is properly flushed with Ar, the current immediately falls to 3×10^{-9} A (3×10^{-10} A at 2 Pa) and vice versa (Figure 8). Due to its reversibility, spin-coated **2** films might be potentially applied as a detector for air humidity. In contrast with previous results, with increasing temperature the current decreases from 4×10^{-7} A at 20 °C until it reaches the local minimum 4×10^{-8} A at 60–70 °C. Finally, from 80 °C upwards the current measured at ambient conditions closely reproduces the current obtained under 2 Pa with constant Ar flux. These results nicely illustrate the reduction in the air humidity content absorbed into the sample with increasing temperature. It seems that the sample should be completely dehumidified at approximately 80 °C.

In summary, we synthesized the conjugate of racemic [6]helicene with an imidazolium moiety leading to the novel helicene salt **2** that was consequently characterized and applied for the construction of experimental semiconductor devices and fully reversible humidity sensor in which a thin layer of **2** was prepared by spin-coating. The combination of an imidazolium ring and helicene backbone complementarily improves its properties in general. Specifically, the imidazolium ring facilitates its solubility in polar solvents and contributes to a higher conductivity of layers of **2** compared to [6]helicene itself.

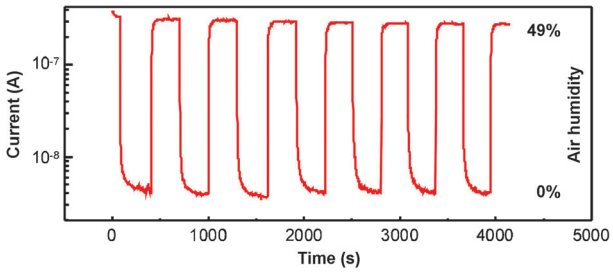

Figure 8. Reversible current dependence on air humidity at a constant voltage (28 V) and temperature 24 °C measured on the thin film of crystalline **2**. The current difference between 0 and 49% air humidity is about two orders of magnitude. The film was exposed to the air humidity (N_2 atmosphere) for 300 s in each step. Similar records were obtained for 3, 5, and 9 V.

Acknowledgements

This work was supported by the grants FR-TI3/628 (J.St.) and FR-TI4/457 (J.V.) from the Ministry of Industry and Trade of the Czech Republic and by the Technology Agency of the Czech Republic (TA04010082, J.St.). M.D. is grateful to Praemium Academiae (ASCR). M.K. would like to thank project CZ.1.07/2.3.00/20.0254 "ReAdMat - Research Team for Advanced Non Crystalline Materials" co-financed by the European Social Fund and the state budget of the Czech Republic. This work was supported by grant OPVK, CZ.1.07/2.3.00/20.0057 from the Czech Ministry of Schools, Youth and Sports (M.Ku.).

Keywords: helicenes · imidazolium salt · organic electronics · organic semiconductor · sensors

[1] E. B. Anderson, T. E. Long, *Polymer* **2010**, *51*, 2447.
[2] A. Monge-Marcet, R. Pleixats, X. Cattoën, M. Wong Chi Man, *Catal. Sci. Technol.* **2011**, *1*, 1544.
[3] N. Noujeim, L. Leclercq, A. R. Schmitzer, *Curr. Org. Chem.* **2010**, *14*, 1500.
[4] R. Ghosh, B. De, *Int. J. Pharm. Sci. Rev. Res.* **2013**, *23*, 237.
[5] R. Sharma, R. K. Mahajan, *RSC Adv.* **2014**, *4*, 748.
[6] M. Gingras, *Chem. Soc. Rev.* **2013**, *42*, 968.
[7] M. Gingras, *Chem. Soc. Rev.* **2013**, *42*, 1051.
[8] M. Gingras, G. Felix, R. Peresutti, *Chem. Soc. Rev.* **2013**, *42*, 1007.
[9] Y. Yang, R. C. Da Costa, M. J. Fuchter, A. J. Campbell, *Nat. Photonics* **2013**, *7*, 634.
[10] Y. H. Tian, G. Park, M. Kertesz, *Chem. Mater.* **2008**, *20*, 3266.
[11] C. Nuckolls, T. J. Katz, L. Castellanos, *J. Am. Chem. Soc.* **1996**, *118*, 3767.
[12] C. Johannessen, E. W. Blanch, C. Villani, S. Abbate, G. Longhi, N. R. Agarwal, M. Tommasini, D. A. Lightner, *J. Phys. Chem. B* **2013**, *117*, 2221.
[13] L. M. Markham, L. C. Mayne, B. S. Hudson, M. Z. Zgierski, *J. Phys. Chem.* **1993**, *97*, 10319.
[14] F. Rodrigues, P. S. Santos, *Vib. Spectrosc.* **2010**, *54*, 123.
[15] L. T. Costa, L. J. A. Siqueira, B. G. Nicolau, M. C. C. Ribeiro, *Vib. Spectrosc.* **2010**, *54*, 155.
[16] Y. Y. Noh, J. Ghim, S. J. Kang, K. J. Baeg, D. Y. Kim, K. Yase, *J. Appl. Phys.* **2006**, *100*.
[17] Y. Y. Noh, D. Y. Kim, K. Yase, *J. Appl. Phys.* **2005**, *98*.

Received: October 31, 2014
Published online on December 11, 2014